Quantum-Mechanical Calculation of Inelastic Cross Sections for $1\,^1S \rightarrow 2\,^3S$ Excitation Collisions of Ground-State He Atoms with He^+ Ions*

S. A. Evans
Texas Instruments, Dallas, Texas 75222

Neal F. Lane†
Physics Department, Rice University, Houston, Texas 77001

(Received 26 December 1972)

Quantum-mechanical, three-state, close-coupling calculations of the inelastic cross sections for $1\,^1S \rightarrow 2\,^3S$ excitation of ground-state He atoms in collision with He^+ ions have been carried out for energies between 25 and 50 eV (c.m.). Differential, partially integrated (over small angles), and total inelastic cross sections were obtained. The calculations were performed using linear combinations of three single-configuration, valence-bond-type electronic wave functions as the basis of a diabatic representation. The diabatic coupling in the vicinity of the well-established $^2\Sigma_g^+$ curve crossing at $R \simeq 1.5a_0$ was found to be small, and it was verified by comparison with the close-coupling results that the Stueckelburg-Landau-Zener (SLZ) theory was applicable. Several SLZ model calculations were performed using the best available adiabatic potential curves and modeling the crossing region. The resulting differential and partially integrated (over small angles) cross sections were found to be in good qualitative agreement with the measurements. In particular, the strange hump apparent in the small-angle cross sections versus energy curve, which was first found by Utterback, and recently confirmed by MacVicar-Whelan and Borst, was reproduced in our calculations. The interesting nature of the small-angle scattering is discussed, and the sensitivity of the cross section to details of the potential curves near the crossing is examined in detail.

I. INTRODUCTION

A. Background

The basic theory of low-energy atom-atom collisions has been available for many years.[1,2] Although this theory has been extended, recast, and elaborated on frequently,[3-7] its application to most diatomic systems is still not well understood. In this paper, we will address ourselves to the problem of applying the theory to a specific system when both theoretical and experimental data are available.

In low-energy collisions, the electronic states of the "quasimolecule" are best represented by perturbed stationary-state functions of some form.[8] These functions, however, will not, in general, be eigenfunctions of the electronic Hamiltonian H_e.[9,10] In this case, transitions will arise from coupling through the off-diagonal elements of the electronic part of the Hamiltonian H_e as well as the familiar nonadiabatic part of the Hamiltonian (sometimes referred to as momentum coupling, or as velocity-dependent or gradient interaction), containing both spherical and angular-dependent terms. Recently, Smith[10] has shown that one can construct in a well-defined manner a set of electronic functions which will cause the spherical nonadiabatic terms to vanish. In this representation, distortion due to the interaction of molecular states is contained entirely in the off-diagonal elements of H_e, which in general are large. In order to be consistent with Smith's development, we will call this the *diabatic representation* (Lichten[11] has used the term "diabatic" when referring to cases in which the off-diagonal elements can be neglected, whereas Levine[12] has called this approximation "diabatic decoupling"). Smith has also pointed out that one can readily define an R-dependent unitary transformation relating the diabatic electronic basis set to the well-known adiabatic basis in which the electronic Hamiltonian is diagonal. In the diabatic representation, the diagonal elements combined with the internuclear repulsion represent somewhat unconventional molecular potential-energy curves which are not subject to the noncrossing rule.[13] In the adiabatic representation, electronic energy curves of like symmetry and quantal description will, of course, repel each other through configuration interaction, and thus avoid crossing in the Born-Oppenheimer approximation.

It is evident from the discussion above that one could calculate collision cross sections in either representation as long as all important coupling terms are retained. In cross-section calculations one chooses a particular representation either to help gain an intuitive understanding of the electronic motion during the collision process or, more often, to simplify the computational difficulties that develop in such problems. For example, in a study of the inelastic $2\,^3S - 2\,^3P$ collisions between metastable and ground-state helium

atoms, Evans, Cohen, and Lane carried out the cross-section calculations in both the diabatic and adiabatic representations. As expected, they obtained identical results. However, in the adiabatic representation, it was found that the nonadiabatic coupling was small and could usually be neglected in calculating the elastic cross sections. The collision process in this case is simply described as one in which the orbital electrons rearrange themselves adiabatically so as to allow the two atoms to follow smooth adiabatic potential-energy curves.

B. He-He$^+$ Problem

The experience gained in the He-He work suggested that a study of a system known to be nonadiabatic would further clarify the role of the diabatic and adiabatic potentials in describing the collision process. The He-He$^+$ scattering problem is ideally suited for this purpose since it is comparatively simple, and has continued to receive considerable attention in the literature.

The possible nonadiabatic nature of the lowest $^2\Sigma_g^+$ potential curve of He-He$^+$ was first suggested by Lichten.[11] Marchi and Smith[14] affirmed his conclusion when they were able to reproduce the magnitude and many aspects of the structure in the elastic differential cross sections observed by Lorents and Aberth[15] using an adiabatic $^2\Sigma_u^+$ potential curve[16] and a reasonable guess for the diabatic-decoupled $^2\Sigma_g^+$ repulsive curve.[17] In a later study, Smith *et al.*[18] were able to identify perturbations in the elastic differential cross section with a particular crossing of the lowest $^2\Sigma_g^+$ curve and the next-highest $^2\Sigma_g^+$ curve. They obtained from their study a value of $1.73a_0$ for the radial separation at the crossing.

A number of *ab initio* calculations of the ground and excited $^2\Sigma_g^+$ states of He-He$^+$ have been carried out in the last ten years.[19-24] They all reported a close approach, or "weakly avoided crossing," of the two lowest adiabatic $^2\Sigma_g^+$ curves in the vicinity of $R = 1.5a_0$. The multiconfiguration calculations have revealed, in addition, a whole series of avoided crossings occurring between the higher $^2\Sigma_g^+$ potential-energy curves.[21-23]

The inelastic effects identified by Marchi and Smith[14] and the avoided crossings found in the *ab initio* potential calculations suggested that the inelastic cross sections for $1^1S \rightarrow 2^3S$ transitions could be significant. The early measurements of Utterback[25] had already suggested that this was the case, and in fact provided early experimental evidence that such an inelastic cross section could be large in the vicinity of threshold. It had been believed by many researchers that the Massey energy criterion was generally applicable, and hence that energies far above threshold would be required for excitation. The work of Novick and his collaborators at Columbia further emphasized the danger of improper application of the Massey criterion and emphasized the importance of "pseudocrossings" of the potential-energy curves.[26] The importance of the $1^1S \rightarrow 2^3S$ cross section near threshold has now been further confirmed by both experiment[25,27,28] and theory.[24,29]

In this paper, we will give the results of an *ab initio* calculation of the three lowest $^2\Sigma_g^+$ molecular potential-energy curves of He-He$^+$ and close-coupling calculations of the $1^1S \rightarrow 2^3S$ inelastic cross section. In the diabatic representation, the diagonal elements of H_e (the diabatic-decoupled potential) were found to exhibit two crossings. In order to study the effect of these crossings on the inelastic trajectories, we carried out a close-coupling calculation of the differential and total cross sections for all possible inelastic transitions within the three-state model. In addition, the Stueckelburg-Landau-Zener[10] (SLZ) semiclassical approximation was applied, using the diabatic matrix elements derived from the two lowest adiabatic $^2\Sigma_g^+$ curves in calculating the differential and total cross section for $^2\Sigma_g^+$ $(1^1S \rightarrow 2^3S)$ transitions. The agreement found between the close coupling and the SLZ results shows that the effective coupling between the two lowest electronic states is confined to a narrow range of internuclear separation R, and that the coupling is relatively weak. Reassured then, of the validity of the semiclassical approximation for this particular application, we have applied the SLZ method and the two-state model, using the more accurate *ab initio* potentials calculated by Michels[21] and Bardsley.[23] The SLZ differential and total inelastic cross sections are compared to the most recent experiments, and are shown to be in semiquantitative agreement. The sensitivity of small-angle scattering to the nature of the potentials in the crossing region has been explored by calculating the partially integrated ($\Theta \leq 5°$ lab), and differential cross section using several different potential models.

II. THEORY

A. General Problem

The general formulation of the low-energy atom-atom collision problem has already been described in some detail by Smith[10] and discussed and applied by Evans *et al.*[9] We will present only highlights of the theory, emphasizing those equations essential to our work.

Using the perturbed-stationary-state approxi-

mation, the total wave function may be expanded in the usual way as

$$\Psi(\vec{R},\vec{r})=\sum_k F_k(\vec{R})\,\chi_k(\vec{R},\vec{r}), \tag{1}$$

where $\chi_k(\vec{R},\vec{r})$ is a member of a complete set of orthonormal electronic functions, $\vec{R}$ is the relative internuclear separation, and $\vec{r}$ labels the internal electron coordinate. Substituting $\Psi(\vec{R},\vec{r})$ into Schrödinger's equation for the di-atom, multiplying by $\Psi^*(\vec{R},\vec{r})$ and integrating over all electron coordinates, the problem is reduced to the solution of a set of coupled equations given by

$$(\underline{T}+\underline{U}-\underline{1}E)\underline{F}(\vec{R})=0\,, \tag{2}$$

where $\underline{U}$ is the familiar potential-energy matrix (atomic units are used throughout). By writing the nuclear momentum operator in a rotating system,[10] the nuclear kinetic-energy matrix may be written as

$$\underline{T}=(1/2\mu)\left[-\underline{1}\nabla_R^2+\underline{S}_R+(1/R^2)\,\underline{S}_\Omega\right], \tag{3}$$

where the second term represents momentum, or velocity-dependent, coupling between states of like spin, symmetry, and angular momentum, and is spherically symmetric. The third term, which possesses angular dependence, couples states which have the same symmetry and spin but which differ in the value of the angular momentum. Since our main concern in this paper is the effect of $^2\Sigma_g^+$ avoided crossings on the inelastic cross section, $\underline{S}_\Omega$ will be ignored. The term $\underline{S}_R$ may also be neglected for reasons given in Sec. II B.

B. Potential-Energy Matrix Elements and Curves

Potential-energy matrix elements of the type required in Eq. (2) must be calculated before attempting to solve the quantum-mechanical scattering equations. The procedure we have used is essentially that developed by the molecular physics group at the University of Texas.

In our close-coupling approximation the wave function in Eq. (1) is truncated to include only the three lowest $^2\Sigma_g^+$ states of the He-He$^+$ system. While our interest is mainly in the diabatic crossing of the two lowest $^2\Sigma_g^+$ states, the third-lowest state is included for several reasons: (*i*) extreme sensitivity of the position of the lowest crossing to the presence of higher $^2\Sigma_g$ states in the expansion, (*ii*) the possibility of observing both diabatic and adiabatic behavior in the same theoretical study, and (*iii*) astrophysical interests in low-energy $^2\Sigma_g^+$ ($2\,^3S\rightarrow 2\,^1S$) transitions.

We have chosen to construct a basis set using single-configuration valence-bond functions. The proper choices for the basis functions ψ_i are properly symmetrized eigenfunctions of the operators $(\vec{S}_a+\vec{S}_b)^2$ and $\vec{S}_{az}+\vec{S}_{bz}$, where a and b label the separated atoms. The symmetrized basis functions may be taken to be

$$\psi_1=d_{11}\,|(1s_b\,1\bar{s}_b'-1\bar{s}_b\,1s_b')1s_a|+d_{12}\,|(1s_b\,2\bar{s}_b-1\bar{s}_b\,2s_b)1s_a|+(a\longleftrightarrow b), \tag{4}$$

$$\psi_2=|1s_b\,2\bar{s}_b\,1s_a|+|1\bar{s}_b\,2s_b\,1s_a|-2\,|1s_b\,2s_b\,1\bar{s}_a|+(a\longleftrightarrow b), \tag{5}$$

$$\psi_3=d_{21}\,|(1s_b\,1\bar{s}_b'-1\bar{s}_b\,1s_b')1s_a|+d_{22}\,|(1s_b\,2\bar{s}_b-1\bar{s}_b\,2s_b)1s_a|+(a\longleftrightarrow b), \tag{6}$$

where $1s_a$ and $1\bar{s}_a$, respectively, denote spin-up and spin-down Slater orbitals centered on nucleus a, the prime on $1s_b'$ denotes an orbital exponent allowed to vary independently from that in $1s_b$, and where the vertical bars denote Slater determinants formed in the usual manner.[30] The constant coefficients d_{ij} were chosen so that ψ_1 and ψ_3 adequately represented the $1\,^1S$ and $2\,^1S$ separated-atom states, respectively, in the limit $R\rightarrow\infty$. The matrix of d coefficients is given by

$$\underline{d}=\begin{bmatrix}1.02214 & -0.06189\\ -0.35818 & 1.08130\end{bmatrix}.$$

There is, of course, no mixing of ψ_2 and ψ_1 or ψ_2 and ψ_3 in the limit $R\rightarrow\infty$ since they represent orthogonal spin states.

At intermediate internuclear separations the ψ_i are taken as basis functions for the calculation of wave functions for the first three $^2\Sigma_g^+$ adiabatic states of He_2^+. Thus for the kth state ($k=1,2,3$) we write

$$\chi_k^a=\sum_{j=1}^{3} C_{kj}\,\psi_j,$$

where the superscript a is appended to remind us that these are approximations to the *adiabatic* electronic wave functions (in contrast to *diabatic* electronic wave functions to be defined later). The linear variational coefficients C_{kj} satisfy the truncated secular equation

$$\sum_{j=1}^{3} C_{kj}(H_{ij}-S_{ij}E_k)=0,\quad i=1,2,3$$

for each root E_k ($k=1,2,3$), where H_{ij} and S_{ij} are the matrix element of the electronic Hamiltonian H_e and the overlap integral, respectively, in the basis ψ_j. A complete variation of the orbital exponents in the Slater-type orbitals was carried out at each internuclear separation so as to minimize the highest root [i.e., the root which correlates with $E(2\,^1S)+E(1\,^1S)$ in the limit $R\rightarrow\infty$]. For

example, the *separated-atom* (actually $R = 20a_0$) energies obtained in this way for the states $He^+ + He(2^1S)$, $He^+ + He(2^3S)$, and $He^+ + He(1^1S)$ are, respectively, −4.1425, −4.1718, and −4.8276 (all in a.u.). [The nonlinear variational parameters in the atomic orbital exponents took on the limiting ($R \to \infty$) values $\zeta_{1s} = 1.97675$, $\zeta_{1s'} = 1.28991$, and $\zeta_{2s} = 0.53596$, where ζ occurs as $e^{(-\zeta r)}$.] In comparison with the corresponding observed energies of −4.1461, −4.1754, and −4.9037, our results do not appear to be very accurate. However, our principal interest is in the nature of the inelastic collision and thus in properties of these wave functions other than the energy. There is no assurance that another significant figure in separated-atom energy would result in "better" wave functions for use in the collision problem. Hence, we were satisfied to proceed with these more modest electronic functions, keeping in mind that *precise* determinations of the cross sections would not be possible.

Since the nonlinear parameters contained in the ψ_i were varied at each internuclear separation R, the basis functions ψ_k take on a weak R dependence. The basis functions may be made orthonormal via a linear transformation

$$\underline{\chi}^d = \underline{A}(R)\underline{\psi}(R) , \tag{7}$$

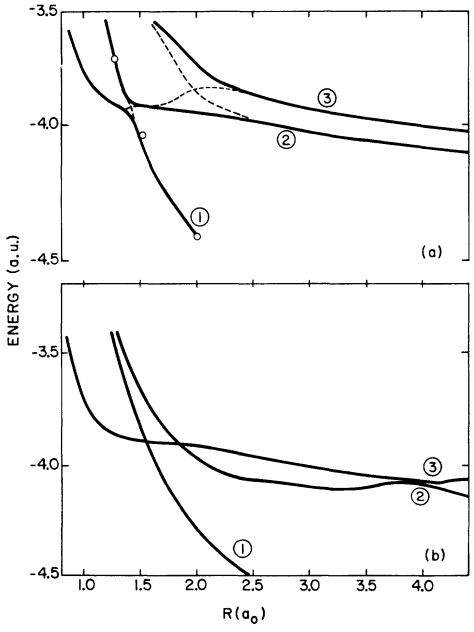

FIG. 1. The three lowest $^2\Sigma_g^+$ potential-energy curves of $He\text{-}He^+$, calculated using three valence-bond single-configuration basis functions. (a) Calculated adiabatic curves U_{ii}^a, $i = 1$, 2, and 3; dashed line—approximate crossing curves; ○, points on the empirical curves (Marchi and Smith); (b) calculated diabatic curves U_{ii}^d, $i = 1$, 2, and 3.

where the matrix $\underline{A}$ contains overlap integrals and is easily determined, and where the three basis functions are treated as elements of a column matrix $\underline{\psi}$. The superscript d will be discussed below. The potential-matrix elements, including nuclear repulsion, are defined for the basis given in Eq. (7) by

$$U_{ij}^d = V_{ij}^d + E_i(\infty)\delta_{ij} = [H_{ij}^d + (4/R)\delta_{ij}] = \int \chi_i^{d*}(H_e + 4/R)\chi_j^d \, d\vec{r} , \tag{8}$$

where H_e is the electronic Hamiltonian and where the $E_i(\infty)$ are the separated-atom limits of the electronic energies. Thus, we have $E_1(\infty) = E(1^1S)$, $E_2 = E(2^3S)$, and $E_3 = E(2^1S)$, relative to ground-state He^+. The weak R dependence present in $\underline{\psi}$ and $\underline{A}$ allows a finite momentum coupling through the second term in Eq. (3). However, since the variation of the nonlinear parameters with R was found to be small in the regions of R where crossings occurred, this weak momentum coupling was neglected. The functions which make up $\underline{\chi}^d$ in Eq. (7) thus qualify as a limited basis set of purely diabatic wave functions, hence the use of the superscript d. These functions are, of course, related to those of the adiabatic representation by an R-dependent unitary transformation of the form

$$\underline{\chi}^a(R) = \underline{C}(R)^{-1}\underline{\chi}^d(R) , \tag{9}$$

where the potential-energy matrix in Eq. (8) is diagonalized by the same transformation, *viz.*

$$\underline{U}^a \equiv \underline{V}^a + \underline{E}(\infty) = \underline{C}^{-1}(R)[\underline{V}^d + \underline{E}(\infty)]\underline{C}(R), \tag{10}$$

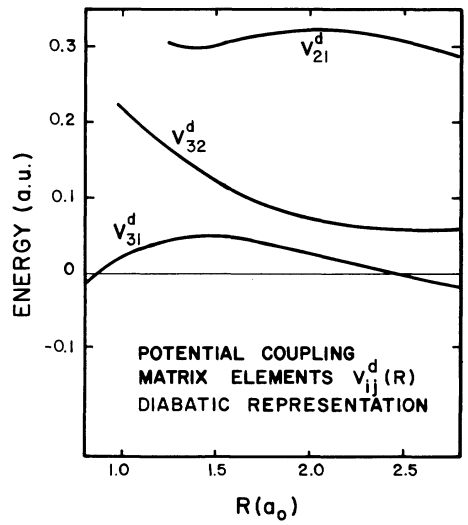

FIG. 2. Diabatic potential-energy coupling matrix elements between the three lowest $^2\Sigma_g^+$ electronic states of $He^+\text{-}He$.

where the matrices $\underline{V}^d$ and $\underline{E}(\infty)$ are defined in Eq. (8). The properties and precise form of $\underline{C}$ are discussed in more detail by Smith.[10]

The potential-energy matrix elements in both representations are given in Fig. 1. As expected, several crossings occur between the diabatic potentials. The diabatic coupling elements are given in Fig. 2. The coupling $V_{31}^d(R)$ is seen to be sufficiently weak in the vicinity of the crossing so as to allow a close approach in Fig. 1 of the adiabatic energy curves $U_{11}^a(R)$ and $U_{22}^a(R)$ at $R \cong 1.5$. If the coupling does not prove to be too weak, we may expect a significant probability for occurrence of the inelastic transition $^2\Sigma_g^+$ ($1^1S \rightarrow 2^3S$). The transition may be viewed as occurring via the nonadiabatic momentum coupling "generated" in the unitary transformation to the adiabatic representation.[9] The stronger coupling $V_{32}^d(R)$, which is spread out over a large region of R, results in strong repulsion between the curves $U_{22}^a(R)$ and $U_{33}^a(R)$ and thus a small probability for the occurrence of either the inelastic transitions $^2\Sigma_g^+(1^1S \rightarrow 2^1S)$ or $^2\Sigma_g^+(2^3S \rightarrow 2^1S)$. It follows then that the most probable "paths" of inelastic scattering are those given schematically by the arrows in Fig. 3.

C. Partial-Wave Analysis

The coupled scattering equations are solved in the diabatic representation where momentum coupling is zero. Making the usual partial-wave expansion, we write the scattering amplitude for an $m \rightarrow n$ transition as

$$f_{nm}(\theta) = \tfrac{1}{2} i(k_n k_m)^{-1/2} \times \Sigma_l (2l+1)[\delta_{nm} - S_{nm}^l] P_l(\cos\theta). \quad (11)$$

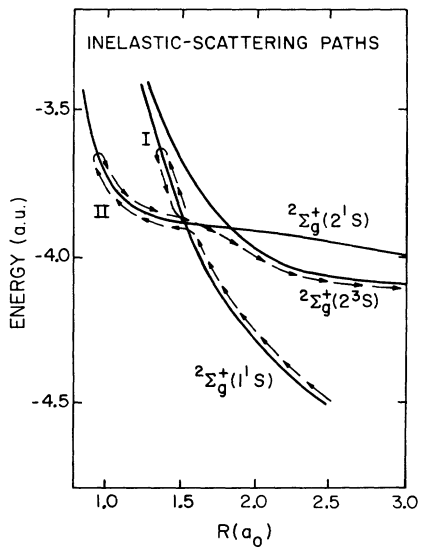

FIG. 3. The two possible inelastic-scattering paths (semiclassical) resulting in $^2\Sigma_g^+$ ($1^1S \rightarrow 2^3S$) transitions.

Similarly, the differential cross section is given by

$$\frac{d\sigma_{nm}(\theta)}{d\Omega} = \frac{k_n}{k_m} |f_{nm}(\theta)|^2 , \quad (12)$$

and the integrated cross section by

$$\sigma_{nm} = (\pi/k_m^2)\Sigma_l (2l+1)|\delta_{nm} - S_{nm}^l|^2. \quad (13)$$

For homonuclear collisions involving two spin-zero bosons (e.g., He^4 atoms), the total wave function must be symmetric under interchange of nuclear spatial coordinates. Imposing this property on the wave function restricts the sums in Eqs. (11) and (13) to even values of l.

D. Procedure

The three second-order coupled differential equations that result from the truncation of the wave function in Eq. (1) are solved numerically using the Numerov algorithm.[9,31] A detailed description of its use in the diabatic representation is given in Ref. 9. It was necessary to deviate slightly from the procedure as discussed there owing to instabilities in solutions for $R \geq 6a_0$. This problem was circumvented by transforming to an adiabatic basis set at $R \cong 5a_0$, using the transformation matrix $\underline{C}(R)$ as defined in Eqs. (9) and (10). The nonadiabatic momentum coupling terms generated by ∇_R^2 in the transformation[9] are neglected, since they are negligible except in the region of a potential crossing.[10,32] In the three-state calculation of the $^2\Sigma_g^+$ potentials given in Fig. 1, no crossings or close approaches occurred beyond $R \cong 4.5a_0$.

III. RESULTS

A. Close-Coupling Three-State Calculation

Using the numerical techniques and the three-configuration *ab initio* potentials discussed above,

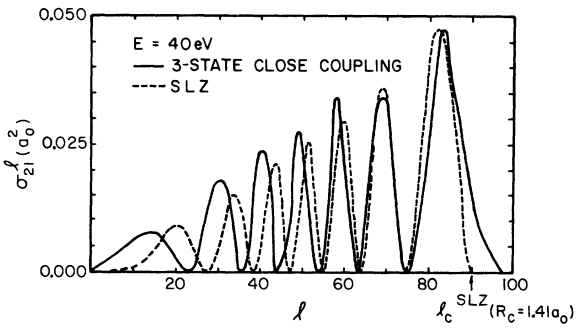

FIG. 4. Partial-wave inelastic cross sections for $^2\Sigma_g^+$ ($1^1S \rightarrow 2^3S$) transition at $E = 40$ eV (c.m.). The total cross section, found by summing over even l, is 0.178 (three-state) and 0.156 (SLZ)$\times 10^{-16}$ cm^2. l_c is the partial-wave angular momentum associated with the curve crossing at $R_c = 1.41a_0$.

we have calculated inelastic cross sections for all possible transitions between the three lowest $^2\Sigma_g^+$ states of He-He$^+$. The total and partial-wave cross sections for $^2\Sigma_g^+(1\,^1S \rightarrow 2\,^3S)$ transitions at $E = 40$ eV are given in Fig. 4. The differential cross section for the same transition and energy is given in Fig. 5. Laboratory measurements of these cross sections are obtained by measuring charge-exchanged He($2\,^3S$) at an angle θ. The low-frequency oscillations are a result of interference between the two possible inelastic scattering paths given in Fig. 3; the higher-frequency oscillations are due to the nuclear symmetry of the diatomic system. It is interesting to note that for $\theta_{\text{c.m.}} \lesssim 25°$ or $\tau \lesssim 1000$ eV deg the inelastic scattering is negligible. This observation can be explained in terms of the classical deflection function Θ, which for the three-state potentials is simply equal to the scattering angle θ. Olsen and Smith[33] have defined for the two possible inelastic-scattering paths the deflection functions

$$\Theta_{\text{I}}^{l}{}_{,\text{II}} = \tfrac{1}{2}[\Theta_a(l, E) \pm \Theta_d(l, E)], \tag{14}$$

where

$$\Theta_a = \tfrac{1}{2}[\Theta_1(l, E) + \Theta_2(l, E)] \tag{15}$$

and

$$\Theta_d = \tfrac{1}{2}[\Theta_1(l, E, r_c) - \Theta_2(l, E, r_c)]. \tag{16}$$

The functions $\Theta_{1,2}(l, E)$ are related to the well-known JWKB phase shift by

$$\Theta(l, E) = 2\,\frac{\partial \eta_l}{\partial_l},$$

whereas the $\Theta_{1,2}(l, E, r_c)$ are special deflection functions defined by

$$\Theta_i(l, E, r_c) = -2l \int_r^{r_c} \left[k_i^{\,2} - u_{ii}(R) - \frac{(l+\tfrac{1}{2})^2}{R^2}\right]^{-1/2} \frac{1}{R^2}\, dR, \qquad i = 1, 2 \tag{17}$$

where r_c is the radius of the crossing, r is the zero of the integrand, and where

$$k_i^2 = 2\mu[E_T - E_i(\infty)],$$

$$u_{ii}(R) = 2\mu[U_{ii}(R) - E_i(\infty)] = 2\mu V_{ii}(R).$$

The function Θ_d reflects the inelastic contribution to the total deflection function resulting from trajectories determined by the potential curves inside the point of curve crossing r_c. The deflection function Θ_{II}^{l}, which will always be smaller than Θ_{I}^{l}, will reach a minimum at l values which correspond to turning points just inside r_c. Using the diabatic crossing potentials given in Fig. 1(a), we found that the elastic contribution Θ_a to the deflection function at $l = 88$ is 45° for $E = 40$ eV. The magnitude of the inelastic contribution Θ_d will depend, through Eqs. (16) and (17), only on the difference between U_{11} and U_{22}. Since in Fig. 5 there is no contribution to the cross section below 25°, we assume that this difference is not large enough to cause scattering at smaller angles. For this particular set of crossing potentials, one can say, qualitatively, that inelastic scattering occurs at internuclear separations too near the scattering center to result in only small changes in trajectory.

Inelastic $^2\Sigma_g^+(1\,^1S,\ 2\,^3S \rightarrow 2\,^1S)$ transitions are inhibited by the strong repulsion between the $^2\Sigma_g^+(2\,^3S)$ and $^2\Sigma_g^+(2\,^1S)$ adiabatic potential curves as shown in Fig. 1. As a result, elastic scattering in the region of the outer diabatic crossing at $R \simeq 1.70a_0$ is adequately described by the adiabatic decoupled potential, as demonstrated in Fig. 6. The cross section for $^2\Sigma_g^+(2\,^3S \rightarrow 2\,^1S)$ transitions in the energy range 30 to 40 eV is of the order 10^{-19} cm^2. The $^2\Sigma_g^+(1\,^1S \rightarrow 2\,^1S)$ was too small to be calculated accurately even in this three-state approximation.

B. Semiclassical Calculation

The close approach of the two lowest $^2\Sigma_g^+$ adiabatic potentials shown in Fig. 1(a), and the abrupt

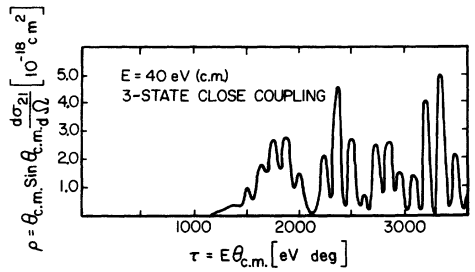

FIG. 5. The differential cross section ρ vs τ for the $^2\Sigma_g^+$ ($1\,^1S \rightarrow 2\,^3S$) transition at $E = 40$ eV (c.m.), calculated using the three-state close-coupling method. ($\theta_{\text{c.m.}}$ is the center-of-mass scattering angle.)

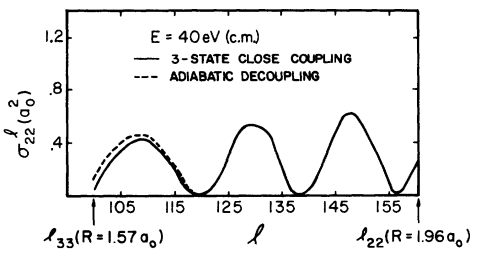

FIG. 6. Elastic partial-wave cross sections for $^2\Sigma_g^+$ ($2\,^3S$) scattering. The calculation is carried out only for values of l associated with turning points in the region of the outermost curve crossing in Fig. 1(b).

cutoff of σ_{21}^{l} at $l \cong 97 (R \cong 1.50 a_0)$ in Fig. 4, strongly suggest a weak-coupling situation in which transitions occur only in a narrow region about the crossing. These are just the assumptions made in deriving the SLZ semiclassical approximation.[10] The SLZ total inelastic-scattering cross section for transitions from state one to state two is given by[3]

$$\sigma_{21}^{SLZ} = (\pi/k_1^2) \Sigma_l (2l+1) |S_{21}^{l}|^2, \tag{18}$$

where

$$|S_{21}^{l}|^2 = 4P_l(1-P_l)\sin^2(\delta_l + \gamma_l),$$
$$P_l = \exp\left[-2\left(\frac{\pi u_{21}^2}{2\mu |u_{11}' - u_{22}'| v_l}\right)\right]_{R=R_c},$$

where the prime denotes differentiation with respect to R and where

$$v_l = \frac{1}{\mu}\left(2\mu[E - E_1(\infty)] - u_{11}(R) - \frac{(l+\frac{1}{2})^2}{R^2}\right)^{1/2}. \tag{19}$$

The probability of a single crossing is P_l, and hence $2P_l(1-P_l)$ is the total probability for a transition from state one to state two. The parameter γ_l is an l-dependent correction to the phase factor

$$\delta_l = \int_r^{r_c} g_+^{1/2}\, dr' - \int_r^{r_c} g_-^{1/2}\, dr',$$

where

$$g_\pm = \tfrac{1}{2}(f_1 + f_2) \pm [(f_1 - f_2)^2 + 4u_{21}^2]^{1/2},$$

with

$$f_{1,2} = k_{1,2}^2 - u_{11,22} - (l+\tfrac{1}{2})^2/r^2.$$

According to Thorson and Boorstein,[34] and Olsen and Smith,[33] the phase correction γ_l has the following properties: $\gamma_l \to -\frac{1}{4}\pi$ as $l \to l_c$, and $\gamma_l \to 0$ as $l \to 0$. We have assumed γ_l to be a small correction, and therefore neglected it for the purposes of this paper. The differential cross section is defined by Eq. (12).

In finding P_l, we set $u_{21}(R) = F(2\mu V_{21})$, where F is a scale factor used to ensure that the energy separation of the adiabatic $^2\Sigma_g^+(1\,^1S)$ and $^2\Sigma_g^+(2\,^3S)$ potential curves at the crossing is 0.0584 a.u., i.e., the same as in the three-state close-coupling calculation. The diagonal elements U_{11} and U_{22} are approximated by smoothly joining the adiabatic potentials $^2\Sigma_g^+(1\,^1S; R > R_c)$ with $^2\Sigma_g^+(2\,^3S; R < R_c)$ and $^2\Sigma_g^+(2\,^3S; R > R_c)$ with $^2\Sigma_g^+(1\,^1S; R < R_c)$. The resulting approximate diabatic, crossing potential-energy curves are plotted in Fig. 1(a) as dotted lines. Had we performed a two-configuration potential-energy calculation, using only the two lowest $^2\Sigma_g^+$ states, the coupling matrix element and the diabatic potentials would have been directly determined within the two-state model; however, the avoided crossing at $R \cong 1.41 a_0$, which is very sensitive to the presence of the higher $^2\Sigma_g^+$ states, would have been very poorly represented. In fact, as we shall show below, three configurations are still not enough to adequately define the details of these potentials in the important region near the crossing.

In Fig. 4 the partial-wave SLZ $1\,^1S \to 2\,^3S$ cross sections are compared with those resulting from the three-state close-coupling calculation at $E =$ 40 eV. The differential $1\,^1S \to 2\,^3S$ cross sections are compared in Figs. 5 and 7. Considering the approximate nature of the diabatic potentials, the agreement is quite good. These results reinforce our assumptions about the characteristics of the crossing, and suggest that a semiclassical calcu-

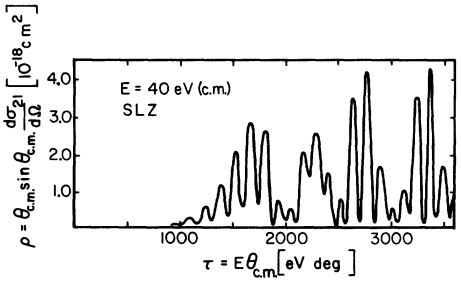

FIG. 7. The differential cross section ρ vs τ for the $^2\Sigma_g^+$ $(1\,^1S \to 2\,^3S)$ transition at $E = 40$ eV (c.m.), calculated using the SLZ method (cf. Fig. 5).

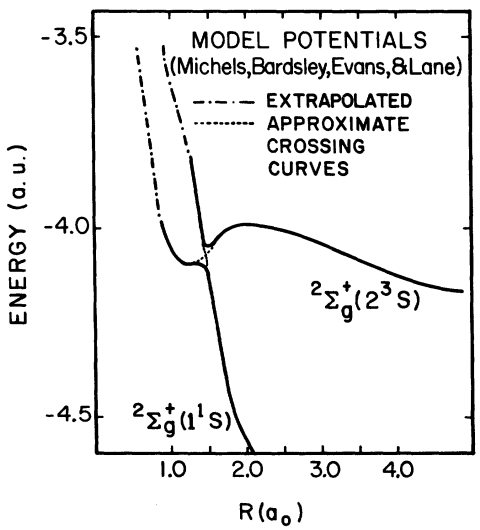

FIG. 8. Model $^2\Sigma_g^+$ potential curves based on the *ab initio* calculations of Michels (Ref. 21), Bardsley (Ref. 23), and Evans and Lane (Ref. 24).

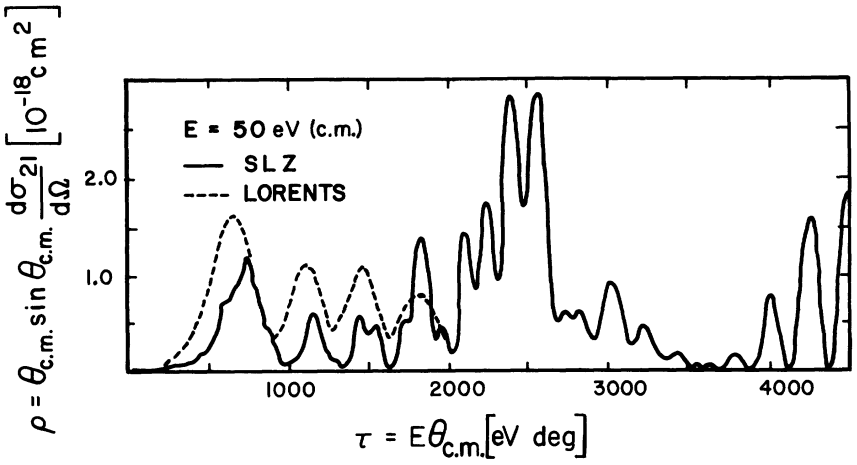

FIG. 9. SLZ differential cross section ρ vs τ for the $^2\Sigma_g^+$ ($1\,^1S \rightarrow 2\,^3S$) transition at $E = 50$ eV (c.m.), calculated using model potentials given in Fig. 8. The dotted line represents the most recent experimental measurements of Lorents (Ref. 28) (cf. Figs. 5 and 7).

lation based on the SLZ approximation may be particularly well suited to this problem.

C. Model Calculation

A comparison of the three-configuration potentials with the multiconfiguration potentials calculated by Michels[21] and Bardsley,[23] shows that the crossing region ($0.25a_0 \lesssim R \lesssim 1.75a_0$) for the two lowest $^2\Sigma_g^+$ states is extremely sensitive to the presence of higher states of the same spin, symmetry, and angular momentum in the wave function. Since the scattering from this region occurs mainly at low angles, the total cross section should be a rather insensitive test of the accuracy of the adiabatic potentials. In this respect, small-angle-scattering data would be very useful in establishing the correct details of the potential curves in the crossing region. In this section, we construct a set of model potentials based on the best available *ab initio* calculations, and by comparing calculated differential cross section at small angles with experimental small-angle-scattering data, test the validity of our choices. The potentials used are those of Michels,[21] modified so that the magnitude of potential coupling (separation of the two $^2\Sigma_g^+$ adiabatic curves) at the crossing radius is approximately equal to that obtained by Bardsley[23] ($2V_{21} = 0.055$ a.u.) and Evans and Lane[24] ($2V_{21} = 0.0584$ a.u.). The diabatic potentials, required in the SLZ calculation, are constructed by joining the appropriate adiabatic curves in the strong-coupling region to obtain the curve crossing. The model potentials in both representations are illustrated in Fig. 8.

The differential cross section calculated at 50 eV, using the model potentials, is given in Fig. 9. The structure is a combination of low-frequency path interference and high-frequency nuclear-symmetry oscillations. Comparison with the experimental measurements of Lorents *et al.*[28] shows that the magnitude of the theoretical cross sections is too small but that the predicted frequency of the interference oscillations is quite good. The resolution of the experiment is too low to see the nuclear-symmetry structure at 50 eV.[29] Unlike the three-state calculations of the differential cross section given in Fig. 5, a significant contribution to the cross section comes from small-angle scattering ($\theta_{c.m.} \lesssim 25°$). From a careful examination of the approximate diabatic curves in Figs. 1 and 8, it is evident that the presence of the higher $^2\Sigma_g^+$ states in the

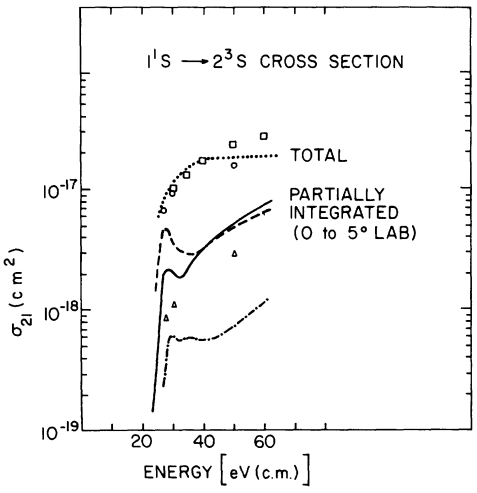

FIG. 10. Total $1\,^1S \rightarrow 2\,^3S$ cross sections: ○, two-state close-coupling (Olson, Ref. 29); □, three-state close-coupling (this work); dotted line, SLZ approximation (this work). Experimental small-angle (0° to 5° lab.) cross sections: dashed line, Utterback (Ref. 25); solid line, McVicar-Whelan and Borst (Ref. 27). Theoretical partially integrated (0° to 5° lab.) cross sections: △, two-state (Olson, Ref. 24); dot-dashed line, three-state (this work).

more accurate potential-curve calculations results in a deeper potential well inside the crossing, giving rise to a larger energy difference between U_{11} and U_{22} in this region. A smaller deflection angle Θ_{II} then results owing to a decrease in the average elastic scattering angle Θ_a and an increase in Θ_d.

The total inelastic cross section for $^2\Sigma_g^+(1\,^1S \rightarrow 2\,^3S)$ transitions is given in Fig. 10. The cross sections measured by Utterback[25] and by McVicar-Whelan and Borst[27] include scattering only into a half-angle of about 5° lab. in the forward direction. In order to compare with these experiments, a partially integrated cross section is obtained by integrating the theoretical differential cross section out to 5° in the lab. system. The partially integrated cross section plotted in Fig. 10 is too small, but it supports the experimental prediction of a peak in the vicinity of 30 eV. If the excitation threshold energy, which is determined by the hump in the model $^2\Sigma_g^+(2\,^3S)$ potential curve, were lowered by 1.7 eV to agree with the experimental threshold energy of about 22.5 eV,[27] the peak in the theoretical cross section would occur at approximately the same energy as that predicted by experiment. Also included in Fig. 10 are the results of model calculations carried out by Olson.[29]

An explanation of the peak in the partially integrated inelastic cross section $[0 \leq \theta \leq 5°(\text{lab.})]$ has been put forward by Olson.[29] Again, discussing the problem in terms of the inelastic deflection function, it can be shown that at very low energies ($E \lesssim 40$ eV) a large difference between U_{11}^d and U_{22}^d will result in a negative deflection function (an attraction instead of a repulsion). In this case, the small-angle scattering receives contributions from both positive and negative branches of Θ_{II}. At higher energies the negative branch is washed out by the centrifugal-force term in the effective potential. The resultant increase in the small-angle scattering is accompanied by additional oscillation in the differential cross section due to the interference of the positive and negative branches of the deflection function. Olson[29] has referred to this effect as the inelastic analog of elastic rainbow scattering. Structure found in the partially integrated inelastic SLZ cross section in the energy range 30–40 eV (Fig. 11) is probably due to interference of the rainbow-scattering oscillations with those due to the nuclear symmetry.

In the experiment of Utterback,[25] a beam containing both metastable and ground-state helium atoms was produced by the charge exchanging of He^+ ions in a beam with He. The beam was then allowed to impact on molecular hydrogen, and the ionization cross section, (i.e., total cross section for production of negative charge) was measured. By also measuring the ionization cross section for fast H_2 molecules impacting on helium atoms, and then taking the difference between the ionization-cross-section curves for He-He_2 and H_2-He in the c.m. system, Utterback obtained a curve proportional to the cross section for the $2\,^3S$ excitation process, where he assumed that the Penning ionization cross section for He*-H_2 collisions is not a strong function of energy. Utterback arbitrarily raised the H_2-He curve 30% in order to make it agree with the He-H_2 curve at higher impact energies. The effect of this correction is to force the cross section for $^2\Sigma_g^+(1\,^1S \rightarrow 2\,^3S)$ transitions to zero for energies $\lesssim 50$ eV center of mass. Since there is no reason for the cross section to go to zero in this energy range, we have neglected the 30% increase in the He-H_2 curve in obtaining the curve plotted in Fig. 10. The reasonable agreement in the slopes of the experimental and theoretical cross sections supports the assumption of a slowly varying Penning ionization cross section within the energy range covered. The absolute value of Utterback's cross section, as given in Fig. 10, should be viewed as uncertain by as much as a factor of 2.[25,35] As given, it assumes the Penning ionization cross section for $He(2\,^3S)$ on H_2 to be of the order 2×10^{-16} cm^2, which is compa-

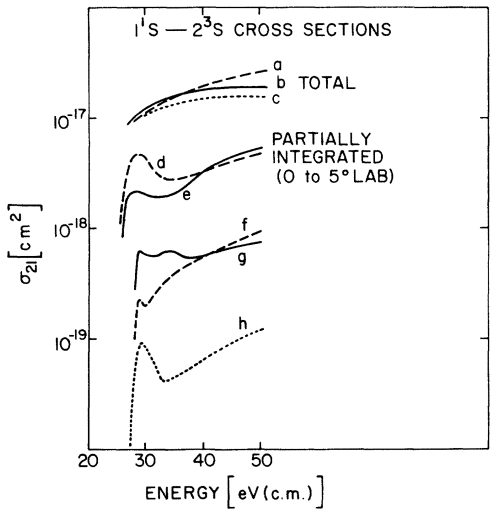

FIG. 11. Total $1\,^1S \rightarrow 2\,^3S$ cross sections in SLZ approximation using potential curves of (a) Michels, (b) model (this work), (c) Bardsley. Experimental small-angle (0° to 5° lab) cross sections: (d) Utterback (Ref. 25), (e) McVicar-Whelan and Borst (Ref. 27). Theoretical SLZ partially integrated (0° to 5° lab) cross sections using potential curves of (f) Michels (Ref. 21), (g) model (this work), (h) Bardsley (Ref. 23).

rable with thermal measurements.[36,37]

In order to demonstrate graphically the sensitivity of small-angle scattering to the detailed nature of the electronic potentials near the crossing, we have calculated the partially integrated SLZ cross section using the unmodified potentials of both Bardsley[23] and Michels[21] in the energy range 28–50 eV. The cross section corresponding to Michel's potentials is especially interesting, since the only essential difference between these and the model potentials given in Fig. 8 is the strength of coupling, which primarily affects the probability of crossing P_l. It is seen in Fig. 11 that the structure observed in the model cross section has disappeared, and that the slope is changed significantly. It can be shown that the partial-wave transition probability

$$2P_l(1-P_l)$$

will have a maximum in the partial-wave range $0<l<l_c$ if the argument of the exponent in Eq. (18) is neither too small nor too large, and that this maximum will shift to larger l as the kinetic energy increases. Also, recalling that each partial-wave angular momentum can be associated in the classical limit with a specific scattering angle (roughly, large $l \rightarrow$ small Θ), we have plotted in Fig. 12 the partial-wave probability using both Michels's *unmodified* potentials and the model potentials at $E=29$ eV. In the case of the model potentials, the peak in the partial-wave transition probability is already located at a large value of l quite near l_c. Hence, a further increase in the energy results in only a small change in the magnitude of the partial-wave transition probability for *large* values of l, and hence a small change in the inelastic scattering at small angles. In contrast, the partial-wave transition probability calculated by using Michels's potentials peaks at $l=0$ for $E=29$ eV. We found that a moderate increase in the energy to 40 eV results in a large shift of the peak to large values of l. Thus at 40 eV, the peak occurs at $l_{max}=75$, where for this case $l_c=102$. This strong energy dependence of the partial-wave transition probability in the region of the crossing is reflected in the partially integrated inelastic cross section as an increase in slope, particularly in the energy range 29–40 eV. In the case of Bardsley's potentials, one could show that the enhanced peak and change in slope is due to the combination of a somewhat different over-all form of the potentials and a different coupling (at the crossing), and hence partial-wave probability of transition.

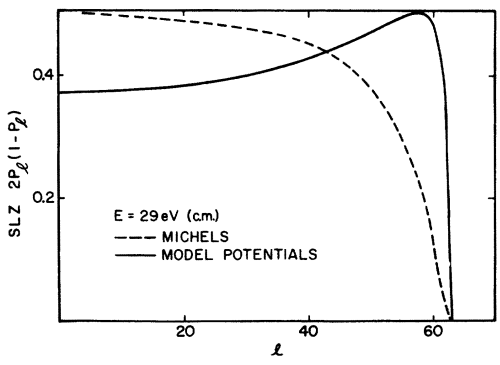

FIG. 12. SLZ total probability of transition from $^2\Sigma_g^+$ ($1\,^1S$) to $^2\Sigma_g^+$ ($2\,^3S$) as a function of l at 29 eV (c.m.).

To investigate the influence of the hump in the $^2\Sigma_g^+(2\,^3S)$ potential on the scattering process, the difference between the maximum and the minimum of the upper $^2\Sigma_g^+$ potential curve was varied. In order to simplify the complicated structure in the differential cross sections, both even and odd partial waves were included in the sum, thus eliminating the high-frequency nuclear-symmetry oscillations. As shown in Fig. 13, an increase in the depth of the potential results in appreciable inelastic scattering at progressively smaller angles. Scattering at large angles is relatively unaffected by these changes since the main contribution is from partial waves l associated with turning points well inside the crossing. In Fig. 13(c), inelastic rainbow interference is clearly visible on the first major peak. This phenomenon is associated with high potential barriers where both positive and negative branches of the deflection function are possible.

IV. SUMMARY AND CONCLUSIONS

In the above work, we have presented results of a three-state *ab initio* calculation of the three low-

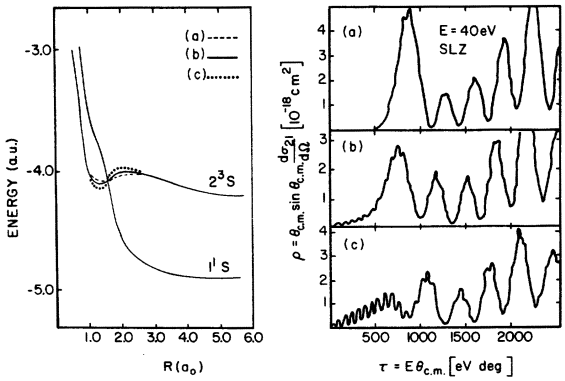

FIG. 13. Inelastic differential cross sections for $^2\Sigma_g^+$ ($1\,^1S \rightarrow 2\,^3S$) transition at 40 eV (c.m.). Cases (a) and (c) represent variations in the hump of the $^2\Sigma_g$ ($2\,^3S$) model potential: (a) dashed line, shallower well and lower maximum; (c) dotted line, deeper well and higher maximum.

est $^2\Sigma_g^+$ electronic states of He_2^+. Two potential-curve crossings occur in the diabatic representation; however, only the inner crossing at $R \cong 1.5a_0$ gives rise to a significant transition probability. Comparison with other more sophisticated multistate *ab initio* calculations of these potential curves has made it clear that the nature of this inner crossing is quite sensitive to the presence of higher $^2\Sigma_g^+$ states.[19-21,23] The three-state close-coupling calculations resulted in inelastic cross sections of the order 10^{-17} cm^2 for $^2\Sigma_g^+(1\,^1S \rightarrow 2\,^3S)$ and 10^{-19} cm^2 for $^2\Sigma_g^+(2\,^3S \rightarrow 2\,^1S)$. The differential inelastic cross section calculated at $E = 40$ eV (c.m.) was found to possess structure due to inelastic-scattering path interference and to nuclear symmetry. The contribution to the inelastic cross section from scattering angles $\theta_{c.m.} \leq 25°$ was found to be negligible. This is due both to the lack of a deep potential well in the upper curve near the crossing and to the nearness of the crossing to the repulsive barrier. Because the coupling between the $^2\Sigma_g^+(1\,^1S)$ and the $^2\Sigma_g(2\,^3S)$ electronic states is confined to a narrow range of values of the internuclear separations near the crossing, we were able to use the semiclassical SLZ approximation in calculating the inelastic cross section. Reasonable agreement between the SLZ cross sections and those found using the three-state close-coupling formulation assured us of the validity of this approximation.

Because of the apparent sensitivity of the inelastic cross section to the detailed nature of the potential curves in the crossing region, we also constructed model potentials based on *ab initio* calculations of Bardsley,[23] Michels,[21] and Evans and Lane.[24] Using these model potentials, we calculated the total and differential $^2\Sigma_g^+(1\,^1S \rightarrow 2\,^3S)$ SLZ inelastic cross sections for several energies between 29 and 60 eV (c.m.). The differential cross section at 40 eV (c.m.) is in qualitative agreement with the experimental results of Lorents.[28] In particular, it contains significant contributions from scattering angles below 25°. Comparison of the partially integrated inelastic cross section with the measurements of Utterback[25] and MacVicar-Whelan and Borst[27] supports the experimental prediction of a peak in the cross section in the vicinity of 30 eV (c.m.). The slopes of partially integrated cross sections calculated by the SLZ method are in good agreement with the measurements. This lends support to the assumption of a slowly varying Penning ionization cross section for He^*-H_2 collisions for energies up to 60 eV. Additional model calculations have revealed that the slope and magnitude of the small-angle inelastic cross section as well as the interference structure depend strongly on the detailed nature of the $^2\Sigma_g^+$ potentials near the crossing.

ACKNOWLEDGMENTS

The authors wish to acknowledge informative discussions with J. C. Browne, R. E. Olson, and N. G. Utterback.

---

*Research supported in part by the U. S. Atomic Energy Commission.

†Alfred P. Sloan Foundation Fellow.

[1]N. F. Mott, Proc. Camb. Philos. Soc. **27**, 553 (1931).
[2]H. S. W. Massey and R. A. Smith, Proc. R. Soc. Lond. **A142**, 142 (1933).
[3]N. F. Mott and H. S. W. Massey, *The Theory of Atomic Collisions*, 3rd ed. (Oxford U. P., London, England, 1965).
[4]H. S. W. Massey, *Electronic and Ionic Impact Phenomena, Slow Collisions of Heavy Particles* (Oxford U. P., London, England, 1971), Vol. 3.
[5]T. F. O'Malley, Adv. At. Mol. Phys. **7**, 223 (1971).
[6]L. Wilets and S. J. Wallace, Phys. Rev. **169**, 84 (1968); J. C. Y. Chen and K. M. Watson, Phys. Rev. **174**, 152 (1968); Phys. Rev. **174**, 188 (1969); Phys. Rev. **174**, 236 (1969); J. C. Y. Chen, C. S. Wang, and K. M. Watson, Phys. Rev. A 1, 1150 (1970).
[7]B. C. Eu, J. Chem. Phys. **52**, 1882 (1970); J. Chem. Phys. **52**, 3903 (1970).
[8]D. R. Bates, H. S. W. Massey, and A. L. Stewart, Proc. R. Soc. Lond. **A216**, 437 (1953).
[9]S. A. Evans, J. S. Cohen, and N. F. Lane, Phys. Rev. A **4**, 2235 (1971); Phys. Rev. A **4**, 2248 (1971).
[10]F. T. Smith, Phys. Rev. **179**, 111 (1969).
[11]W. Lichten, Phys. Rev. **131**, 229 (1963); Phys. Rev. **139**, A27 (1965); Phys. Rev. **164**, 131 (1967).
[12]R. D. Levine, J. Chem. Phys. **49**, 51 (1968).
[13]J. Von Neumann and E. Wigner, Z. Phys. **30**, 467 (1929).
[14]R. P. Marchi and F. T. Smith, Phys. Rev. **139**, A1025 (1965).
[15]D. C. Lorents and W. Aberth, Phys. Rev. **139**, A1017 (1965).
[16]P. N. Reagan, J. C. Browne, and F. A. Matsen, Phys. Rev. **132**, 304 (1963).
[17]E. Phillipson, Phys. Rev. **125**, 1981 (1962).
[18]F. T. Smith, D. C. Lorents, W. Aberth, and R. P. Marchi, Phys. Rev. Lett. **15**, 742 (1965).
[19]J. C. Browne, J. Chem. Phys. **45**, 2707 (1966).
[20]B. K. Gupta and F. A. Matsen, J. Chem. Phys. **47**, 4860 (1967).
[21]H. H. Michels, Natl. Bur. Stds. Tech. Note No. 438, edited by M. Krauss (U.S. GPO, Washington, D.C., 1967), p. 109.
[22]H. Rosenthal and H. M. Foley, Phys. Rev. Lett. **23**, 1480 (1969).
[23]J. N. Bardsley, Phys. Rev. A **3**, 1317 (1971).
[24]S. A. Evans and N. F. Lane, Bull. Am. Phys. Soc. **15**, 1507 (1970).
[25]N. G. Utterback, Phys. Rev. Lett. **12**, 295 (1964).
[26]S. Dworetsky, R. Novick, W. W. Smith, and N. Tolk, Phys. Rev. Lett. **18**, 939 (1967); S. H. Dworetsky and R. Novick, Phys. Rev. Lett. **23**, 1484 (1969).

[27]P. J. MacVicar-Whelan and W. L. Borst, Phys. Rev. A **1**, 314 (1970).
[28]D. C. Lorents (private communication); D. Coffey, Jr., D. C. Lorents, and F. T. Smith, *Proceedings of the Sixth International Conference on the Physics of Electronics and Atomic Collisions: Abstracts* (MIT Press, Cambridge, Mass., 1969), p. 299.
[29]R. E. Olson, Phys. Rev. A **5**, 2094 (1972).
[30]D. R. Scott, E. M. Greenwalt, J. C. Browne, and F. A. Matsen, J. Chem. Phys. **44**, 298 (1966).
[31]D. Hartree, *The Calculation of Atomic Structures* (Wiley, New York, 1957).
[32]D. Levine, B. R. Johnson, and R. B. Bernstein, J. Chem. Phys. **50**, 1964 (1969).
[33]R. E. Olson and F. T. Smith, Phys. Rev. A **3**, 1607 (1971).
[34]W. R. Thorson and S. A. Boorstein, in *Proceedings of the Fourth International Conference on the Physics of Electronic and Atomic Collisions: Abstracts* (Science Bookcrafters, Hastings-on-Hudson, N.Y., 1965), p. 218.
[35]N. G. Utterback (private communication).
[36]R. D. Rundel and R. F. Stebbings, in *Case Studies in Atomic Collision Physics*, edited by E. W. McDaniel and M. R. C. Mc Dowell (North-Holland, Amsterdam, 1972), Vol. 2, p. 547.
[37]R. F. Stebbings (private communication).